Evaluating the Effects of River Partial Penetration on the Occurrence of Riparian Freshwater Lenses

Amir Jazayeri[1,2], Adrian D. Werner[1,2], Huiqiang Wu[3,4], and Chunhui Lu[3,4]

[1]School of the Environment, Flinders University, GPO Box 2100, Adelaide, SA 5001, Australia.

[2]National Centre for Groundwater Research and Training, Flinders University, GPO Box 2100, Adelaide, SA 5001, Australia.

[3]State Key Laboratory of Hydrology-Water Resources and Hydraulic Engineering, Hohai University, China.

[4]Yangtze Institute for Conservation and Development, Hohai University, Nanjing, China.

Corresponding author: Amir Jazayeri (amir.jazayeri@flinders.edu.au)

Key Points:

- New method developed to find saltwater discharge and steady-state, non-dispersive riparian lens shape close to a partially penetrating river
- Consistency between analytical and numerical results highlight the capability of proposed methodology.
- Assumption of a fully penetrating river likely leads to significant overestimates of lens size and saltwater discharge to the river.

Abstract

Previous studies of freshwater lenses in saline aquifers adjoining gaining rivers ("riparian lenses") have so far considered only rivers that fully penetrate the aquifer, whereas in most cases, rivers are only partially penetrating. This paper presents a new methodology for obtaining the saltwater discharge and the shape of a steady-state, non-disperive riparian lens, where the river is partially penetrating, combining two previous analytical solutions. The resulting analytical solution is compared to numerical modelling results to assess assumptions and the methodology adopted to approximate the "turning effect", which is the change in groundwater flow direction (horizontal to vertical) near the partially penetrating river. A range of conditions are analysed, constrained by parameters adopted previously for River Murray floodplains (Australia). Consistency between analytical and numerical results highlight the capability of the proposed analytical solution to predict the riparian lens geometry and saltwater discharge into partially penetrating rivers. The sensitivity analysis indicates that larger riparian lenses are produced adjacent to the deeper and wider rivers, as expected. The change in width or depth of the river has more influence on the saltwater discharge and the horizontal extent of the riparian lens (and less effect on the vertical extent of the lens adjacent to the river) for shallower and narrower rivers. This research highlights the utility of the new method and demonstrates that the assumption of a fully penetrating river likely leads to significant overestimation of the saltwater discharge to the river and the riparian lens horizontal extent and vertical depth.

1 Introduction

Buoyant freshwater lenses may occur in riparian zones and within floodplains adjoining freshwater rivers traversing saline aquifers, which are commonly encountered in arid or semi-arid regions (e.g. Cartwright et al., 2010; Cendón et al., 2010; Werner & Laattoe, 2016; Laattoe et al., 2017). These freshwater lenses (i.e. termed "riparian lenses" in this paper) are of great importance in sustaining riparian and floodplain ecosystems, and in the management of river water quality during low-flow periods (e.g. Holland et al., 2009; Telfer et al., 2012). Riparian lenses have been observed under both losing and gaining river conditions. For example, Cartwright et al. (2010), Alaghmand et al. (2014), and Alaghmand et al. (2015) found riparian lenses under losing river conditions in semi-arid floodplains adjacent to the River Murray, Australia. Riparian lenses were encountered by Munday et al. (2006) under gaining river conditions in geophysical surveys conducted in the Bookpurnong floodplain, also adjacent to the River Murray.

Werner and Laattoe (2016) showed that gaining-river riparian lenses are caused by buoyancy effects. They derived an analytical solution for the shape of these types of lenses (and for the corresponding saltwater discharge rates) that was verified by Werner et al. (2016) through laboratory experimentation. Werner (2017) subsequently added a correction term to the analytical solution of Werner and Laattoe (2016) to correct for the dispersive mixing that was neglected in assuming of freshwater-saltwater immiscibility.

Previous studies of Werner and Laattoe (2016), Werner et al. (2016) and Werner (2017) presumed that the gaining freshwater river penetrates the entire depth of the aquifer. However, it is clear in geological and geophysical-survey cross-sections that the floodplains where riparian lenses were first encountered contain rivers that are incised only partly through the host aquifer (e.g. Munday et al., 2006). The effect of this partial penetration on riparian lenses has not been studied previously.

Miracapillo and Morel-Seytoux (2014) showed that the depth of river penetration within an aquifer is an important controlling factor in estimating river-aquifer exchange flow rates. When a river partially penetrates an aquifer, the direction of groundwater flow to the river bottom may be effectively vertical, thereby violating the Dupuit-Forchheimer (D-F) assumption of zero resistance to vertical flow used in earlier methods for calculating river-aquifer interactions that adopt a fully penetrating river (e.g. Hantush, 1965). To overcome errors introduced by the change in groundwater flow direction (from horizontal to vertical), Morel-Seytoux (2009) introduced a "turning factor", which, simply put, is a factor that modifies the river-aquifer connectivity that would otherwise apply to a fully penetrating river, thereby accounting for the resistance caused by the change in flow direction in the vicinity of a partially penetrating river (a more detailed explanation and mathematical application of the turning factor is provided later in this article). This followed the earlier work of Morel-Seytoux (1975), who proposed river loss influence coefficients for incorporating the effect of river penetration. Morel-Seytoux et al. (2014) provided a table of coefficients (from curve-fitting of analytical values) that allow for the application of simple formula to obtain the turning factor. They considered the case of a river placed at the land surface (i.e. does not penetrate the aquifer). Miracapillo and Morel-Seytoux (2014) modified this approach to account for partial penetration of the aquifer by the river, and added an approach for calculating the river-aquifer exchange when the heads on the two sides of the river are different (i.e. asymmetric riparian heads).

In this study, the riparian lens theory of Werner and Laattoe (2016) is combined with the river partial-penetration theory provided by Morel-Seytoux (2009), Miracapillo and Morel-Seytoux (2014), and Morel-Seytoux et al. (2014) to produce a methodology for estimating riparian lenses adjacent to partially penetrating rivers that are gaining. This is expected to broaden the applicability of previous riparian lens solutions that apply only to fully penetrating, gaining rivers.

2 Theory

This section combines two previous analytical solutions to produce a new methodology for obtaining the saltwater discharge and the geometry of a steady-state riparian lens adjacent to a gaining river, which partially penetrates an otherwise saline aquifer. Figure 1 depicts the corresponding conceptual model, showing the buoyant riparian lens. The riparian lens is presumed to contain stagnant groundwater, and therefore, the watertable is horizontal. The river width of $2W_r$ [L] is bisected under the assumption of symmetry. The river penetrates to a depth η_r [L] into the aquifer and receives steady-state saline groundwater discharge q_s [L^2T^{-1}] (i.e. discharge per unit length of river perpendicular to the cross-section). Resistive material of thickness B_r [L] lines the river, and the depth of the aquifer base below the riverbed is η_a [L]. Freshwater and saltwater thicknesses are designated η_f [L] and η_s [L], respectively. The riparian lens extends to a distance x_L [L] from the origin (point "*o*", aligned with the riverbank edge and the base of the aquifer; Figure 1). Here, at the lens tip, the saltwater thickness is η_{sL} [L]. The saltwater thickness at the origin (i.e. adjacent to the riverbank) is η_{sr} [L], and η_{sb} is the saltwater thickness at the landward boundary (or at least the location of a known head or flux of saltwater towards the river, e.g. from a monitoring well), located at x_b [L].

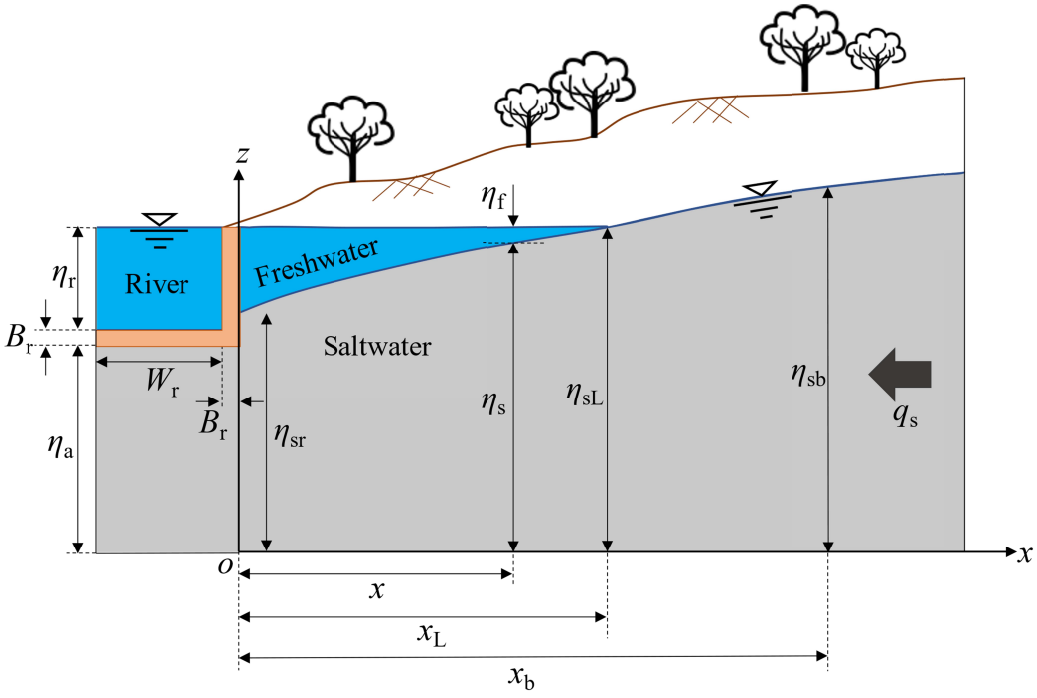

Figure 1. Conceptual model of saline groundwater flow to a partially penetrating river with a riparian lens adjacent to the river. The river is bisected along an axis of symmetry. Blue and grey shading represent freshwater and saltwater, respectively.

Morel-Seytoux (2009) presumed that groundwater flow in an aquifer adjacent to a partially penetrating river is effectively horizontal at some "far distance" from the river, given here as x_B [L], whereas closer to the river, the flow has a non-negligible vertical component. The D-F assumption presumably holds for $x \geq x_B$. Previous studies have presumed that the D-F assumption applies beyond distances from the river equal to twice the aquifer thickness or average aquifer thickness (e.g. Haitjema, 1987; Morel-Seytoux, 2009; Morel-Seytoux et al., 2014, 2017), at least for freshwater-only situations. Applying this notion to the current riparian lens situation, the value of x_B was taken as $2d_s$, where d_s [L] is the average thickness of saltwater between the riverbank and at distance x_B. That is:

$$d_s = \frac{\eta_{sr} + \eta_{sB}}{2} \tag{1}$$

Here, η_{sB} [L] is the saltwater thickness at x_B, and η_{sr} is shown in Figure 1.

Flow to the river incorporates the turning factor of Morel-Seytoux (2009). That is, the exchange flow between the river and aquifer is proportional to the difference in head between the river and a point in the aquifer sufficiently distant from the river to allow the D-F assumption to apply (i.e. at $x = x_B$), given for freshwater-only conditions as (Morel-Seytoux, 2009):

$$Q = KL\Gamma\left(h_r - h_B\right) \tag{2}$$

where Q [L^3T^{-1}] is the fresh groundwater flow to each side of the river, K [LT^{-1}] is the aquifer hydraulic conductivity (in this case, for freshwater), L [L] is the river reach length (perpendicular to the river cross-section), Γ [-] is the one-side dimensionless conductance, h_r [L] is the head in the river, and h_B [L] is the head in the aquifer at x_B.

Equation (2) needs modification to apply to the conceptual model of Figure 1 because of the effects on flow of having two fluids (freshwater and saltwater) of different densities. To account for saltwater flow beneath a buoyant riparian lens, equation (2) is modified to express head variables in equivalent saltwater head terms, in a similar manner to Werner and Laattoe (2016), as:

$$q_s = K_s \Gamma_s \left(h_{sr} - h_{sB} \right) \tag{3}$$

Here, L in equation (2) is taken as unity, reducing Q to q_s. K_s [LT^{-1}] is the saltwater hydraulic conductivity of the aquifer, which relates to the freshwater K through $K_s = \rho_s \mu_f K/(\rho_f \mu_s)$, where ρ_s and ρ_f are saltwater and freshwater densities [ML^{-3}] and μ_s and μ_f are freshwater and saltwater dynamic viscosities [$ML^{-1}T^{-1}$], respectively. For simplicity, $\mu_f/\mu_s = 1$ is adopted. Γ_s [-] is the modified, one-side, dimensionless conductance for saltwater flow, which is defined in Section 2.3. h_{sr} and h_{sB} [L] are equivalent hydrostatic saltwater heads at the river and at x_B, respectively. The former is given by:

$$h_{sr} = \eta_a + B_r + \frac{\rho_f}{\rho_s} \eta_r \tag{4}$$

h_{sB} depends on whether x_B is beyond or within the extent of the riparian lens, as discussed in subsections that follow.

2.1 Scenario 1: x_B within the riparian lens area ($x_B < x_L$)

Where the riparian lens exists ($x \le x_L$; Figure 1), the combined thickness of the lens and underlying saltwater is equal to the height of the river water level above the aquifer base, namely:

$$\eta_s + \eta_f = \eta_{sL} = \eta_a + B_r + \eta_r \tag{5}$$

Within the area of the lens where the D-F assumption is valid ($x_B \le x \le x_L$), the saltwater head that drives (saltwater) flow is equal to the depth of saltwater flow (η_s) plus the saltwater head caused by the (freshwater) riparian lens, giving rise to an equivalent saltwater head (h_s [L]) of:

$$h_s = \eta_s + \frac{\rho_f}{\rho_s} \eta_f \tag{6}$$

Combining equations (5) and (6) produces:

$$h_s = \eta_s + \frac{\rho_f}{\rho_s} \left(\eta_a + B_r + \eta_r - \eta_s \right) \tag{7}$$

Noting that at x_B, $h_s = h_{sB}$, and $\eta_s = \eta_{sB}$, and combining equations (3), (4) and (7) leads to:

$$q_s = K_s \Gamma_s \left(1 - \frac{\rho_f}{\rho_s}\right)\left(\eta_a + B_r - \eta_{sB}\right) \tag{8a}$$

And:

$$\eta_{sB} = \eta_a + B_r - \frac{q_s}{K_s \Gamma_s \left(1 - \frac{\rho_f}{\rho_s}\right)} \tag{8b}$$

Where the D-F assumption is applicable ($x \geq x_B$), saltwater flow (i.e. q_s) can be described by Darcy's law for horizontal flow:

$$q_s = -K_s \eta_s \frac{dh_s}{dx} \tag{9}$$

Beyond the extent of the lens ($x \geq x_L$), q_s is given by:

$$q_s = -K_s \eta_s \frac{d\eta_s}{dx} \tag{10}$$

By taking the definite integration of equation (10) between two arbitrary points, x_1 and x_2, where $x_L \leq x_1$, $x_2 \leq x_b$, then:

$$q_s \left(x_2 - x_1\right) = -\frac{K_s}{2}\left(\eta_{s2}{}^2 - \eta_{s1}{}^2\right) \tag{11}$$

Substituting $x_1 = x_L$, $\eta_{s1} = \eta_{sL}$, $x_2 = x_b$ and $\eta_{s2} = \eta_{sb}$ into equation (11), q_s can be found as:

$$q_s = -\frac{K_s}{2\left(x_b - x_L\right)}\left(\eta_{sb}{}^2 - \eta_{sL}{}^2\right) \tag{12a}$$

And:

$$x_L = \frac{K_s}{2q_s}\left(\eta_{sb}{}^2 - \eta_{sL}{}^2\right) + x_b \tag{12b}$$

The equation for saltwater flow beneath the lens, for region $x \geq x_B$, can be obtained by substituting equation (7) into equation (9), producing (Werner & Laattoe, 2016):

$$q_s = -K_s \left(1 - \frac{\rho_f}{\rho_s}\right)\eta_s \frac{d\eta_s}{dx} \tag{13}$$

The definite integral of equation (13), between x_1 and x_2, where $x_B \leq x_1$, $x_2 \leq x_L$ becomes:

$$q_s \left(x_2 - x_1\right) = -\frac{K_s}{2}\left(1 - \frac{\rho_f}{\rho_s}\right)\left(\eta_{s2}{}^2 - \eta_{s1}{}^2\right) \tag{14}$$

Substituting $x_1 = x_B$, $\eta_{s1} = \eta_{sB}$, $x_2 = x_L$ and $\eta_{s2} = \eta_{sL}$, equation (14) becomes:

$$q_s = -\frac{K_s}{2(x_L - x_B)}\left(1-\frac{\rho_f}{\rho_s}\right)\left(\eta_{sL}^{\,2} - \eta_{sB}^{\,2}\right) \tag{15}$$

Seeking q_s as a function of variables that can be measured in field situations, we eliminate η_{sB} and x_L by combining equations (8b), (12b) and (15), resulting in the following quadratic equation:

$$aq_s^{\,2} + bq_s + c = 0 \tag{16}$$

where coefficients a, b and c are given by:

$$a = -\frac{1}{K_s\Gamma_s^2\left(1-\frac{\rho_f}{\rho_s}\right)} \tag{17a}$$

$$b = 2\left(x_b - x_B + \frac{(\eta_a + B_r)}{\Gamma_s}\right) \tag{17b}$$

$$c = K_s\left(\eta_{sb}^{\,2} - \frac{\rho_f}{\rho_s}\eta_{sL}^{\,2} - \left(1-\frac{\rho_f}{\rho_s}\right)(\eta_a + B_r)^2\right) \tag{17c}$$

Equation (16) can easily be solved to obtain q_s, and the lens extent, x_L is then attainable from equation (12b).

2.2 Scenario 2: x_B outside the riparian lens area ($x_B > x_L$)

When x_B is located outside the riparian lens area, the saltwater head at x_B is equal to the saltwater thickness (i.e. $h_{sB} = \eta_{sB}$), which in combination with equations (3) and (4) produces:

$$q_s = K_s\Gamma_s\left(\eta_a + B_r + \frac{\rho_f}{\rho_s}\eta_r - \eta_{sB}\right) \tag{18a}$$

And:

$$\eta_{sB} = \eta_a + B_r + \frac{\rho_f}{\rho_s}\eta_r - \frac{q_s}{K_s\Gamma_s} \tag{18b}$$

In addition, in the saltwater region, by substituting $x_1 = x_B$, $\eta_{s1} = \eta_{sB}$, $x_2 = x_b$ and $\eta_{s2} = \eta_{sL}$ into equation (11), q_s can be obtained as:

$$q_s = -\frac{K_s}{2(x_b - x_B)}\left(\eta_{sb}^{\,2} - \eta_{sB}^{\,2}\right) \tag{19}$$

Substituting equation (18b) into equation (19) leads again to a quadratic expression in the form of equation (16), where coefficients a, b and c are given by:

$$a = \left(\frac{1}{K_s\Gamma_s}\right)^2 \tag{20a}$$

$$b = \frac{-2}{K_s}\left(x_b - x_B + \frac{\left(\eta_a + B_r + \frac{\rho_f}{\rho_s}\eta_r \right)}{\Gamma_s} \right) \tag{20b}$$

$$c = \left(\eta_a + B_r + \frac{\rho_f}{\rho_s}\eta_r \right)^2 - {\eta_{sb}}^2 \tag{20c}$$

The value of q_s can again be achieved by solving equation (16), allowing x_L to be obtained from equation (12b).

2.3 Modified, one-side, dimensionless conductance for saltwater flow to the river (Γ_s)

Morel-Seytoux (2009) showed, for freshwater-only problems, that Γ is a function of the normalized wetted perimeter, W_p^N [-], and the normalised degree of penetration, d_p^N [-] of the river. W_p^N is W_p/d, where W_p is the wetted perimeter of the river and d is the average aquifer thickness, or simply the aquifer thickness. d_p^N is η_r/d. Modification of the method for obtaining Γ is required to account for the buoyant riparian lens. That is, W_p^N is replaced with a saltwater normalised wetted perimeter (W_{sp}^N [-]), which we define as:

$$W_{sp}^N = \frac{W_{sp}}{d_s} = \frac{2\left(W_r + \left(\eta_{sr} - \eta_a - B_r\right)\right)}{d_s} \tag{21}$$

where W_{sp} is the total wetted perimeter through which saltwater discharges (on both sides of the river). d_p^N is replaced with a saltwater normalised degree of penetration (d_{sp}^N [-]), given by:

$$d_{sp}^N = \frac{\eta_{sr} - \eta_a - B_r}{d_s} \tag{22}$$

By using W_{sp}^N and d_{sp}^N obtained from equations (21) and (22), instead of W_p^N and d_p^N for freshwater-only situations, Γ_s can be calculated by the following steps. Firstly, the value of Γ_s for the situation of no river penetration or a flat recharge zone (i.e. Γ_{flat} [-]) is calculated from (Morel-Seytoux et al., 2014):

$$\Gamma_{flat} = \frac{1}{2\left[1 + \frac{1}{\pi}\ln\left(\frac{2}{1 - \sqrt{e^{-\pi W_{sp}^N}}}\right)\right]} \tag{23}$$

Secondly, Γ_{flat} is adjusted to account for partial penetration of the river (Miracapillo & Morel-Seytoux, 2014):

$$\Gamma_p = \Gamma_{flat}\left[1 + a_1 d_{sp}^N + a_2\left(d_{sp}^N\right)^2\right] \tag{24}$$

where a_1 [-] and a_2 [-] are given in Table 1.

Table 1. Values for partial penetration coefficients in equation (24), given by Morel-Seytoux et al. (2014).

W_{sp}^N range	d_{sp}^N range	a_1	a_2
$W_{sp}^N \le 1.0$	$d_{sp}^N \le 0.2$	0.890	-2.430
$W_{sp}^N \le 1.0$	$0.2 < d_{sp}^N \le 0.5$	0.538	-0.387
$1.0 < W_{sp}^N \le 3.0$	$d_{sp}^N \le 0.2$	0.819	-1.340
$1.0 < W_{sp}^N \le 3.0$	$0.2 < d_{sp}^N \le 0.5$	0.672	-0.542
$1.0 < W_{sp}^N \le 3.0$	$0.5 < d_{sp}^N \le 0.9$	0.567	-0.330

Finally, a modification to the conductance is required if a clogging layer exists (Morel-Seytoux, 2009):

$$\Gamma_c = \frac{\Gamma_p}{\left(1 + 2\left(\frac{B_r}{W_{sp}}\right)\left(\frac{K_s}{K_{sc}}\right)\Gamma_p\right)} \tag{25}$$

Here, K_{sc} [LT^{-1}] is the saltwater hydraulic conductivity of the clogging layer. Thus, Γ_s is either Γ_p or Γ_c depending on the existence of a clogging layer.

2.4 Applying the analytical solution

Calculating q_s using the analytical solution obtained in this study requires knowledge of the position of x_B relative to x_L, which is dependent on q_s via equation (12b), and q_s is determinable from knowledge of the boundary conditions and other measurable parameters according to equations (16) and (17a-c) or (20a-c) (the choice of which depends on the position of x_B relative to x_L). Hence, solving for q_s and x_L requires iteration of the theory given earlier.

Several assumptions were used to approximate the initial values required to start the iteration process. Firstly, $d_s \approx \eta_a$ (and hence $x_B \approx 2\eta_a$) was adopted. Secondly, the values of W_{sp}^N and d_{sp}^N required to calculate Γ_s were approximated by $W_{sp} \approx 2W_r$ (i.e. assuming that ($\eta_{sr} - \eta_a - B_r$) << W_r), and the equivalent saltwater depth within the river (i.e. $\eta_r\rho_f/\rho_s$) was chosen as a replacement for ($\eta_{sr} - \eta_a - B_r$) in equation (22), leading to the following initial estimates:

$$W_{sp}^N \approx \frac{2W_r}{\eta_a} \tag{26}$$

$$d_{\mathrm{sp}}^{N} \approx \frac{(\rho_{\mathrm{f}}/\rho_{\mathrm{s}})\eta_{\mathrm{r}}}{\eta_{\mathrm{a}}} \tag{27}$$

Using equations (26) and (27), the initial value of Γ_s can be calculated from equations (23) to (25). Thirdly, it was assumed that $x_B < x_L$, and therefore the initial value of Γ_s is used in equations (17a-c) to find the coefficients in equation (16). Note that the solution to equation (16) to find q_s has two roots, only one of which is acceptable; namely the negative root indicating saltwater flow towards the river.

The value of q_s is then applied in equation (12b) to calculate x_L. The value of x_L is compared with x_B to check if the initial assumption of $x_B < x_L$ was correct or not. If $x_B > x_L$, equations (20a-c) should be used to calculate the coefficients of equation (16). The new value of q_s can be obtained by finding the negative root of equation (16), which is used in equation (12b) to find a new value for x_L. The obtained values of q_s and x_L can be used to find η_{sB} through application of equation (8b) (if $x_B < x_L$) or equation (18b) (if $x_B > x_L$). Values of q_s and x_L also allow for the calculation of η_{sr} using equation (14) (by substituting $x_1 = 0$, $\eta_{s1} = \eta_{sr}$, $x_2 = x_L$ and $\eta_{s2} = \eta_{sL}$). The corrected values of variables d_s, x_B, W_{sp}, W_{sp}^{N} and d_{sp}^{N} can be calculated from the obtained values of η_{sr} and η_{sB} through equation (1) (to find d_s), equation (21) (to find W_{sp}^{N}) and equation (22) (to find d_{sp}^{N}). Then, the above method is repeated to find new values of Γ_s, q_s, x_L, η_{sr} and η_{sB}. The iteration procedure needs to be continued until convergence criteria are met. We ceased iterating once the change in q_s between two consecutive iterations was less than 0.1%.

After finding the converged values of q_s and x_L, the freshwater-saltwater interface can be tracked using equation (14) by adopting $x_1 = x$, $\eta_{s1} = \eta_s$, $x_2 = x_L$ and $\eta_{s2} = \eta_{sL}$, as:

$$\eta_{\mathrm{s}} = \sqrt{\frac{2q_{\mathrm{s}}\left(x_{\mathrm{L}} - x\right)}{K_{\mathrm{s}}\left(1 - \dfrac{\rho_{\mathrm{f}}}{\rho_{\mathrm{s}}}\right)} + {\eta_{\mathrm{sL}}}^{2}} \tag{28}$$

The iteration procedure required to apply the above analytical solution is summarised as a flowchart in Figure 2.

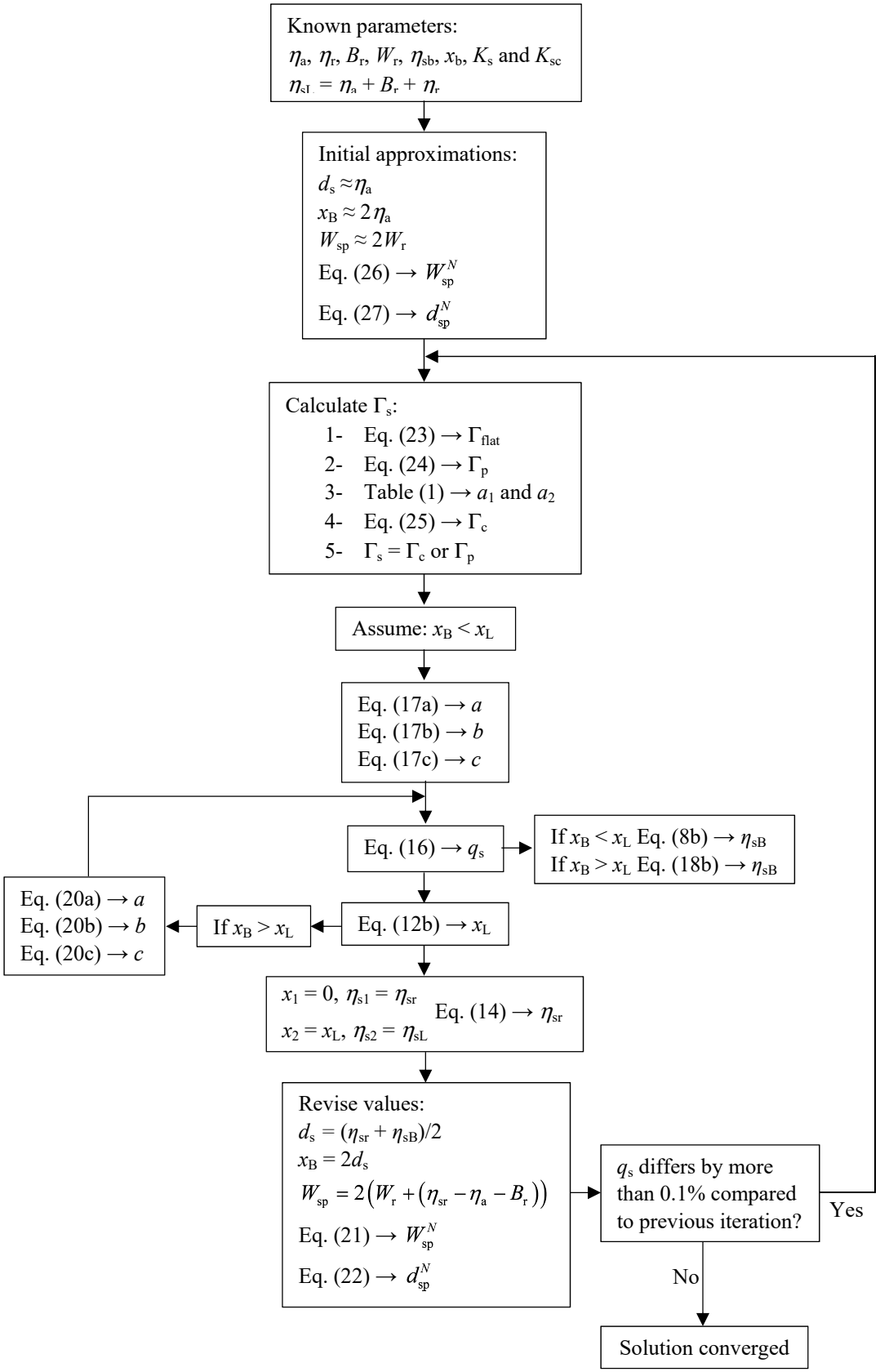
Known parameters:
η_a, η_r, B_r, W_r, η_{sb}, x_b, K_s and K_{sc}
$\eta_{sL} = \eta_a + B_r + \eta_r$
Initial approximations:
$d_s \approx \eta_a$
$x_B \approx 2\eta_a$
$W_{sp} \approx 2W_r$
Eq. (26) → W_{sp}^N
Eq. (27) → d_{sp}^N
Calculate Γ_s:
1- Eq. (23) → Γ_{flat}
2- Eq. (24) → Γ_p
3- Table (1) → a_1 and a_2
4- Eq. (25) → Γ_c
5- $\Gamma_s = \Gamma_c$ or Γ_p
Assume: $x_B < x_L$
Eq. (17a) → a
Eq. (17b) → b
Eq. (17c) → c
Eq. (16) → q_s
If $x_B < x_L$ Eq. (8b) → η_{sB}
If $x_B > x_L$ Eq. (18b) → η_{sB}
Eq. (12b) → x_L
If $x_B > x_L$
Eq. (20a) → a
Eq. (20b) → b
Eq. (20c) → c
$x_1 = 0$, $\eta_{s1} = \eta_{sr}$
$x_2 = x_L$, $\eta_{s2} = \eta_{sL}$
Eq. (14) → η_{sr}
Revise values:
$d_s = (\eta_{sr} + \eta_{sB})/2$
$x_B = 2d_s$
$W_{sp} = 2\left(W_r + \left(\eta_{sr} - \eta_a - B_r\right)\right)$
Eq. (21) → W_{sp}^N
Eq. (22) → d_{sp}^N
q_s differs by more than 0.1% compared to previous iteration?
Yes
No
Solution converged

253

Figure 2. Flowchart of iteration method for applying the partially penetrating riparian lens analytical solution ("Eq." means "Equation").

It should be noted that equation (28) is based on the D-F assumption, which is presumed to hold for the region $x_B \leq x \leq x_L$. For the region $0 \leq x < x_B$, where a component of vertical flow is expected, equation (28) is also used to deduce the lens shape, including η_{sr}, in the absence of an alternative formula for the lens shape in this near-river region. This introduces some errors in the analytical solution for the near-river part of the lens ($0 \leq x < x_B$) that are assessed in Section 3. Even though lens calculations for $0 \leq x < x_B$ do not comply with the D-F assumption, any error associated with that non-compliance does not necessarily influence other calculations within the analytical approach (e.g. calculated values of x_L and q_s).

3 Comparison to numerical modelling

3.1 Description of model setup

Numerical modelling of partially penetrating rivers lined with low-K streambed material was undertaken using SEAWAT (version 4; Langevin et al., 2008) to evaluate the analytical solution proposed herein. SEAWAT has been extensively used and validated for variable-density flow and solute transport, combining MODFLOW-2000 (Harbaugh et al., 2000) and MT3DMS (Zheng & Wang, 1999) through the water density term. For brevity, the mathematical formulation of SEAWAT is not shown here and the reader is referred to the software documentation (Guo & Langevin, 2002).

Various river geometries (width and depth of penetration) were tested using cross-sectional simulations of an unconfined aquifer. The vertical extent of the numerical model domain for all cases was constant at 10 m, while the horizontal extent was varied from 95 to 99 m to obtain the same distance between the riverbank edge and the landward boundary (i.e. 90 m), despite different W_r. The numerical models adopt the cell widths ranging from 0.19 to 0.198 m and a depth of 0.2 m, leading to a total of 25,000 cells. This achieved a balance between accuracy of the results and reasonable computational run times, which were up to one hour on a quadcore Intel® Core™ i5-7500 processor.

The saltwater boundary was represented by specified-head boundary condition, while the freshwater river was simulated using the General-Head Boundary (GHB) package of SEAWAT (Langevin et al., 2008). Use of the GHB package allowed flow into or out of the model domain (via the river) depending on the resistance of a clogging layer, represented by the boundary conductance. Specifically, following the guidance given in (Harbaugh et al., 2000) the GHB conductance (C_{GHB} [L^2T^{-1}]) was set to:

$$C_{GHB} = \frac{KK_c\Delta A}{\left(KB_r + K_c\frac{\Delta L}{2}\right)} \quad (29)$$

where ΔA [L^2] is the cell cross-sectional area perpendicular to the flow. For horizontal GHB cells along the horizontal river bottom, $\Delta A = \Delta x \Delta y$ and for the vertical riverbank, $\Delta A = \Delta z \Delta y$, where Δx, Δz and Δy (Δy is perpendicular to the river cross-section and is equal to 1 m) are the cell size [L] in x, z and y (perpendicular to the river cross-section) directions, respectively. ΔL [L] is the

cell size in the direction of flow (i.e. Δz and Δx for GHB cells representing the parts of the river boundary that are horizontal and vertical, respectively).

Figure 3 illustrates an example of the model boundary conditions and river geometry, representing Case E-4 in the current study.

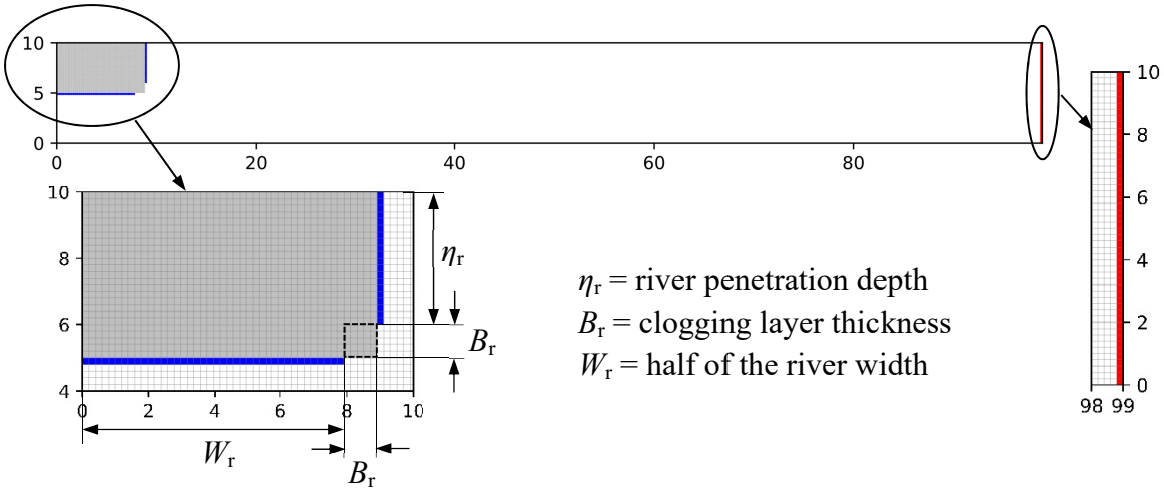

Figure 3. An example of model domain (for Case E-4; described in Table 3). Red, blue and grey cells represent specified-head (saltwater; solute concentration = 1), general-head (freshwater; solute concentration = 0) and no-flow (inactive) boundary conditions, respectively. The black dashed lines in the lower right corner of the incised area where, conceptually, the clogging layer does not abut river water. A more detailed explanation for the lack of GHB boundary cells (blue) along the lower-right corner of the inactive zone is offered in the main text. Units are in metres.

Figure 3 shows that GHB boundary cells are not used to represent the entire perimeter of the incised area in the top left corner of the model, which represents the physical space occupied by the river and surrounding riverbed materials. This is because the GHB boundary cells represent the connection of the aquifer to the river through riverbed material. The GHB cells simulate river-aquifer connection that occurs perpendicular to the riverbed (horizontal river bottom) and the riverbank (vertical side of the river). Therefore, as the clogging layer in the lower right corner of the incised region does not connect the aquifer to water river (perpendicular to the boundary), we omitted any connectivity between the aquifer and the river along the outer edge of these cells (i.e. there are no GHB cells along this part of the perimeter). An alternative to this approach could have been to try to parameterise GHB cells in this region considering the convergent flow that might occur through the corner square of riverbed material, i.e., towards the lower right corner of the river. This would have required a rather arbitrary choice of conductance (which would have been lower than the value used along other parts of the boundary where flow to the river is perpendicular to the riverbank/riverbed), so we prefer simply to disconnect the aquifer from the river where there is not a connection to the aquifer in the direction perpendicular to the river boundary. This resulted in vertical and horizontal lengths of the incised region equal to B_r where no GHB cells were placed (i.e. the square region shown by black dashed lines in Figure 3), while GHB cells covered a horizontal distance of W_r and a vertical distance of η_r,

corresponding with the river width and depth, respectively. Also, preliminary model testing found that a better match to the analytical solution was obtained with the approach to GHB cell distribution in Figure 3.

Solute concentrations at specified-head and general-head boundaries were dealt with in the Sink and Source Mixing (SSM) package of MT3DMS (Zheng & Wang, 1999). This allowed groundwater discharge to occur at the ambient salt concentration, and incoming groundwater to have specified salinity levels (e.g. freshwater in the case of the river and saltwater at the inland boundary). The SEAWAT models were run in transient mode until steady-state conditions were achieved, as indicated by time-invariant total solute mass in the model. Periods needed to reach steady-state conditions were in the order of 5000 to 8000 days.

The parameters adopted in numerical models (and corresponding analytical solutions, where parameters are relevant) were chosen to be consistent with previous studies (e.g. Werner, 2017) and are considered reasonable for River Murray conditions (i.e. consistent with parameter ranges provided by Werner and Laattoe (2016) for typical River Murray conditions). Parameter values are given in Table 2.

Table 2. Parameters used in numerical and analytical models.

Parameter	Symbol	Value	Unit
Aquifer freshwater hydraulic conductivity[a]	K	10	m/d
Clogging layer freshwater hydraulic conductivity[a]	K_c	1	m/d
Clogging layer thickness	B_r	1	m
Freshwater density	ρ_f	1000	kg/m^3
Saltwater density	ρ_s	1025	kg/m^3
Distance of landward boundary from riverbank	x_b	90	m
Saltwater thickness at landward boundary	η_{sb}	10.05	m
Specific yield[b]	S_y	0.24	–
Specific storage[b]	S_s	10^{-6}	1/m
Effective porosity[b]	n	0.3	–

[a]SEAWAT uses K and K_c as input, while K_s and K_{sc} should be adopted in the analytical solution.

[b]Parameter used only in numerical models.

Dispersion parameters in numerical models (i.e. longitudinal dispersivity, α_L [L], transverse dispersivity, α_T [L], and molecular diffusion, D_m [L^2T^{-1}]) were set to zero as an attempt to simulate non-dispersive, sharp-interface conditions (or at least minimal dispersion). However, some dispersion occurred in SEAWAT due to unavoidable artificial numerical dispersion (Werner, 2017).

Twenty cases were used to consider various river geometries, including river widths and depths varying from 4 to 8 m and 1 to 4 m, respectively. These river geometries correspond to

351 W_{sp}^{N} and d_{sp}^{N} ranging from 0.95 to 2.40 and 0.05 to 0.15, respectively. Table 3 provides the
352 parameters for various river geometries used in analytical and numerical models.

353

354 **Table 3.** Parameters for various river geometries adopted in numerical and analytical models.

River depth	η_r (m)		1	2	3	4
Depth of aquifer beneath riverbed base	η_a (m)		8	7	6	5
River half-width	W_r (m)	4	A-1	A-2	A-3	A-4
		5	B-1	B-2	B-3	B-4
		6	C-1	C-2	C-3	C-4
		7	D-1	D-2	D-3	D-4
		8	E-1	E-2	E-3	E-4

355

356 3.2 Analytical solution and numerical simulation results and comparison

357 The steady-state salinity distributions of numerical models and the sharp-interface of the
358 analytical solution for various river geometries are shown in Figure 4, with key results listed in
359 Table 4, which also contains the discrepancies in the three main riparian lens characteristics (i.e.
360 q_s, x_L and η_{sr}). Here, numerical results for x_L and η_{sr} are compared to the analytical solution by
361 considering the 0.5 relative salinity concentration (i.e. 50% saltwater concentrations) isochlor
362 from numerical models.

363

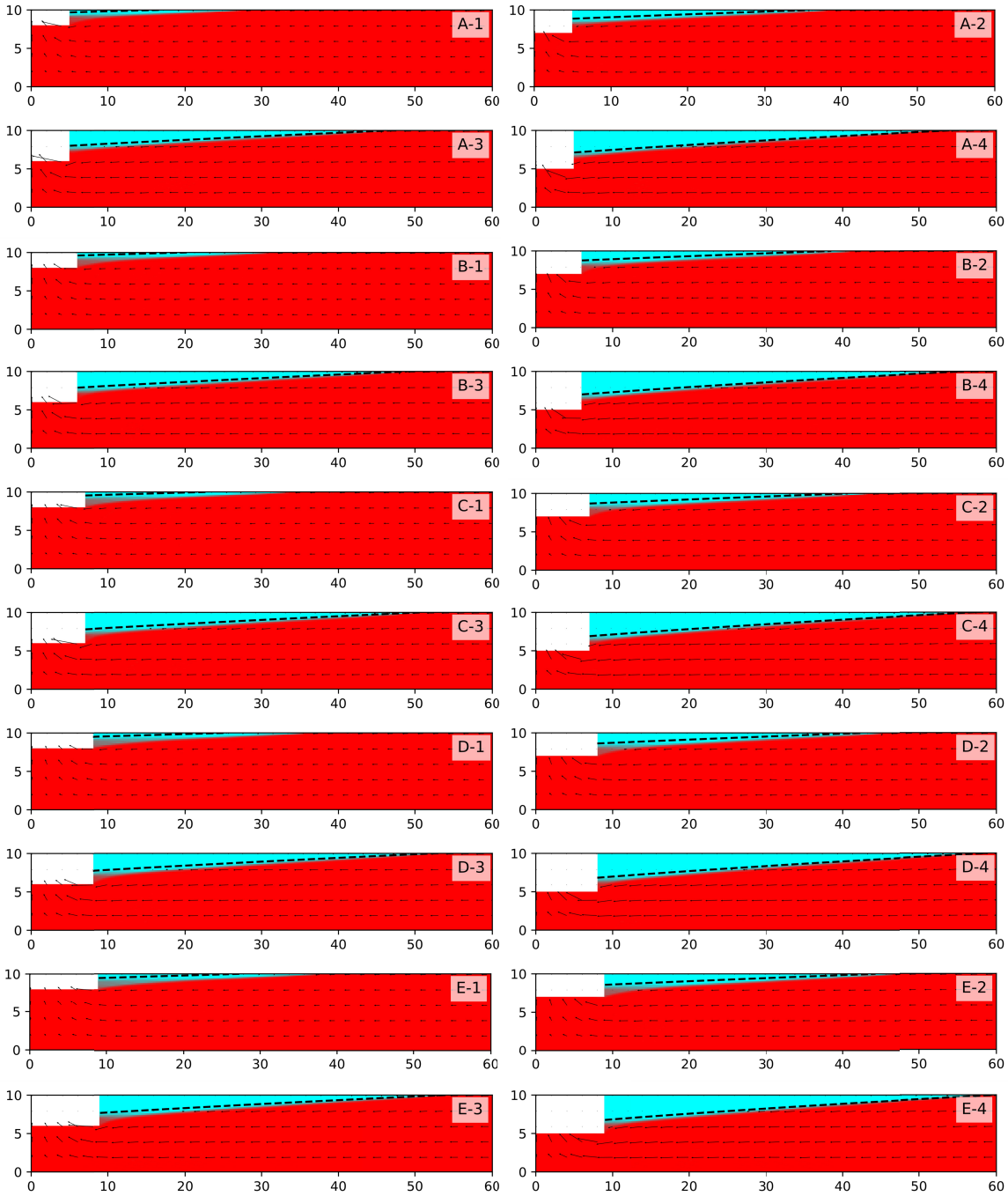

364

365 **Figure 4.** Comparison between numerical model salinity distributions (cyan and red are
366 freshwater and saltwater, respectively) and sharp-interface tracked line (black dashed line) from
367 analytical solution. Arrows indicate the velocity vectors from numerical simulations (one in ten
368 vectors is shown). An explanation of each case is given in Table 3. Units are in metres and
369 salinity varies from 0 (freshwater) to 1 (saltwater). Note that only a portion of the model domain
370 (60 m from the river centre) is shown for clarity.

371

372 **Table 4.** Numerical and analytical model results of q_s, x_L and η_{sr} for different cases.

	Numerical model[a]			Analytical solution			Difference[b] (%)		
Case	q_s (m^2/s)	x_L (m)	η_{sr} (m)	q_s (m^2/s)	x_L (m)	η_{sr} (m)	q_s	x_L	η_{sr}
A-1	-0.0834	23.10	9.10	-0.0656	11.69	9.69	-21.3	-49.4	6.43
A-2	-0.102	35.03	8.27	-0.0869	30.89	8.86	-14.7	-11.8	7.21
A-3	-0.119	42.63	7.48	-0.107	41.94	8.01	-10.3	-1.61	7.10
A-4	-0.135	47.98	6.69	-0.125	49.01	7.13	-7.14	2.16	6.66
B-1	-0.0868	25.24	9.01	-0.0678	14.21	9.61	-21.9	-43.7	6.60
B-2	-0.106	36.60	8.12	-0.0894	32.50	8.76	-15.3	-11.2	7.87
B-3	-0.123	43.91	7.30	-0.109	43.05	7.89	-10.9	-1.96	8.08
B-4	-0.138	49.00	6.50	-0.128	49.81	7.00	-7.64	1.65	7.78
C-1	-0.0892	27.03	8.87	-0.0695	16.03	9.54	-22.2	-40.7	7.63
C-2	-0.108	37.70	8.02	-0.0912	33.69	8.68	-15.6	-10.7	8.29
C-3	-0.125	44.81	7.18	-0.111	43.87	7.80	-11.2	-2.09	8.68
C-4	-0.141	49.69	6.37	-0.130	50.40	6.91	-7.89	1.43	8.46
D-1	-0.0910	28.45	8.70	-0.0708	17.40	9.49	-22.3	-38.9	9.08
D-2	-0.110	38.44	7.94	-0.0927	34.58	8.62	-15.8	-10.0	8.63
D-3	-0.127	45.40	7.09	-0.113	44.50	7.73	-11.3	-1.98	9.04
D-4	-0.143	50.14	6.27	-0.131	50.86	6.83	-7.96	1.44	8.85
E-1	-0.0920	32.31	8.45	-0.0718	18.45	9.46	-22.0	-42.9	11.9
E-2	-0.111	38.88	7.89	-0.0939	35.27	8.57	-15.5	-9.28	8.64
E-3	-0.128	45.70	7.04	-0.114	45.00	7.67	-11.0	-1.55	9.04
E-4	-0.144	50.40	6.22	-0.133	51.22	6.76	-7.65	1.62	8.65

373 [a]Based on 0.5 relative salinity concentration (i.e. 50% saltwater concentrations) isochlor.

374 [b](analytical result − numerical result)/numerical result × 100%.

375

376 The numerical and analytical results given in Figure 4 and Table 4 indicate that shallow
377 rivers produce much smaller riparian lenses than those adjacent to rivers that penetrate almost the
378 entire aquifer thickness, thus highlighting the benefit of the partially penetrating solution. The
379 proposed analytical solution provides a reasonable prediction of the riparian lens geometry and
380 saltwater discharge into partially penetrating rivers for the majority of cases. For example,
381 differences between numerical simulations and analytical results has a maximum of 22% for q_s,
382 which was obtained for the case of the smallest river penetration depth (i.e. η_r = 1 m; Cases A-1,
383 B-1, C-1, D-1 and E-1). In other cases, q_s discrepancies are less than 16%. Table 4 shows that the
384 analytical solution tends to underestimate the magnitude of q_s in all cases.

385 In terms of x_L, the analytical solution and numerical models differ by less than 12% for
386 all cases except those with river depths of 1 m (i.e. Cases A-1, B-1, C-1, D-1 and E-1), for which
387 significant analytical-numerical discrepancies were obtained (39-49%). We attribute these high
388 errors to the stronger vertical flows that arise in the cases with the shallowest rivers (i.e. smallest
389 η_r of 1 m), leading to the largest departures from the D-F assumption adopted in the analytical
390 solution. Lens extents were underestimated by the analytical solution, relative to numerical
391 results, in 15 of the 20 cases listed in Table 4.

392 Analytical-numerical differences in η_{sr} were less than 12% in all cases, and were
393 overestimated by the analytical solution. Therefore, riparian lenses obtained using the new
394 method are deeper but extend a shorter distance from the riverbank compared to those from
395 numerical models.

396 Statistical criteria, including mean absolute error (MAE), root mean square error
397 (RMSE), percent bias (PBIAS) and Nash-Sutcliffe efficiency (NSE) (Moriasi et al., 2007), are
398 presented in Table 5 to evaluate the match between analytical solution and numerical
399 simulations. MAE, RMSE, PBIAS values closer to 0 and NSE closer to 1 indicate better
400 agreement (Moriasi et al., 2007). The sign of PBIAS values in Table 5 indicate that the analytical
401 solution underestimates both q_s and x_L, while η_{sr} was overestimated (as described above). These
402 statistics considered together suggest that the analytical and numerical models are generally in
403 reasonable agreement.

404

405 **Table 5.** Statistical criteria to evaluate analytical-numerical model agreement.

	q_s	x_L	η_{sr}
MAE	0.0151(m^2/s)	4.31 (m)	0.63 (m)
RMSE	0.0154 (m^2/s)	6.21 (m)	0.64 (m)
PBIAS (%)	13.1	9.85	-8.21
NSE	0.37	0.47	0.52

406

407 Figure 5 represents the results of sensitivity analysis using the analytical solution, in
408 which the sensitivity of q_s, x_L, η_{sr} and η_{sB} to changes in W_r and η_r are shown. The results show
409 that river penetration depth plays a more important role than the river width, in terms of the
410 effect on all four output variables. Increasing η_r (i.e. depth of river penetration) from 1 to 4 m led
411 to larger $|q_s|$ and x_L, while the values of η_{sr} and η_{sB} decreased (i.e. the depth of the lens increased),
412 signifying larger riparian lenses next to deeper rivers, as expected. Deepening the river from 1 to
413 4 m increased q_s by an average of 87% and x_L by an average 231%, while η_{sr} decreased by an
414 average of 28%, and η_{sB} decreased by an average of 20%. The results also indicate that the river
415 penetration depth has a larger effect on q_s and x_L for narrower rivers, while the river penetration
416 depth has almost the same impact on η_{sr} and η_{sB} for different values of W_r.

417

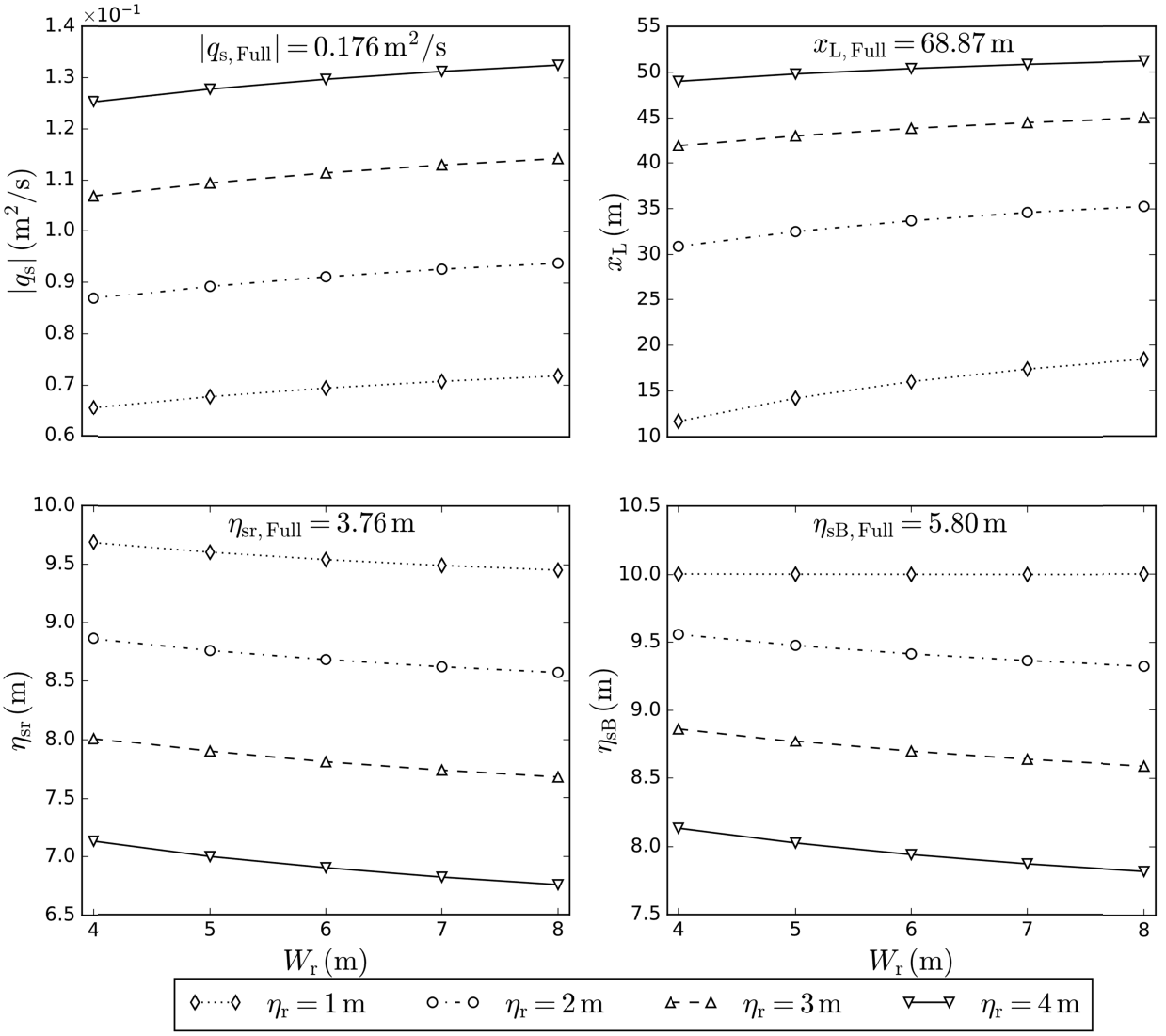

Figure 5. Sensitivity analysis of riparian lens characteristics to river geometries. $|q_{s,\,Full}|$, $x_{L,\,Full}$, $\eta_{sr,\,Full}$ and $\eta_{sB,\,Full}$ represent the corresponding value of q_s, x_L η_{sr} and η_{sB} for a fully penetrating river, respectively.

Figure 5 illustrates that by increasing W_r, larger q_s and x_L were obtained, while η_{sr} and η_{sB} decreased. That is, wider rivers are expected to have more extensive riparian lenses. Widening the river (increasing W_r) from 4 to 8 m increased q_s by an average of 7% and x_L was larger by an average of 21%, while η_{sr} and η_{sB} were smaller by 4% and 2%, on average. This indicates that W_r has a larger effect on q_s and x_L for shallower rivers, while the effect of W_r on η_{sr} and η_{sB} was almost independent of η_r.

Values of $|q_{s,\,Full}|$, $x_{L,\,Full}$, $\eta_{sr,\,Full}$ and $\eta_{sB,\,Full}$, representing a fully penetrating river, are also given in Figure 5 (formulae for fully penetrating rivers given by Werner and Laattoe (2016) and omitted here for brevity). As expected, the assumption of a fully penetrating river for situations

involving partially penetrating rivers may lead to significant overestimates of q_s and x_L, and underestimates of η_{sr}.

4 Conclusions

Previous analytical models for the shape of riparian lenses in saline aquifers (adjacent to gaining rivers) have presumed that the river penetrates the entire aquifer depth. However, we introduce a new methodology for calculating the saltwater discharge and the shape of the riparian lens adjoining a gaining river that partially penetrates an otherwise saline aquifer. The derived analytical solution is solved through an iterative procedure, and is verified by comparison to numerical simulation.

The results of the proposed analytical solution, in terms of the lens extent and saltwater discharge, were in reasonable agreement with numerical modelling values. However, the departure from the D-F assumption near the river for cases involving the shallowest rivers introduced some errors in the lens geometry. This took the form of shorter lenses and less saltwater discharge.

The assumption of a fully penetrating river (when the river is in reality partially penetrating) leads to larger riparian lenses in both horizontal extent and vertical depth. Also, fully penetrating rivers involve greater saltwater discharge compared to partially penetrating rivers.

Differences between numerical and analytical models were, on average, 14% for saltwater discharge and 13% for the lens' horizontal extent. The analytical solution tended to underestimate both saltwater discharge and the horizontal extent of the lens.

Sensitivity analysis, based on the proposed analytical solution, shows that larger riparian lenses are produced adjacent to deeper and wider rivers, as expected. The river depth is more influential factor on the saltwater discharge and the horizontal extent of the lens compared to the river width, for the cases that we considered. Changing the width or depth of the river had more influence on the saltwater discharge and the horizontal extent of the lens for shallower and narrower rivers. The proposed analytical methodology provides a useful screening tool for examination of the occurrence of riparian lens in the floodplain saline aquifer adjacent to gaining river of partial penetration to the aquifer.

Acknowledgements

The authors are thankful for helpful discussions with Hubert Morel-Seytoux (Hydroprose International Consulting) regarding his analytical methodology on river-aquifer exchange fluxes for partially penetrating rivers. Adrian Werner is the recipient of an Australian Research Council Future Fellowship (project number FT150100403). Amir Jazayeri is funded by the Australian Research Council (project numbers FT150100403 and LP140100317). Chunhui Lu acknowledges the financial support from the National Key Research Project (2018YFC0407200), National Natural Science Foundation of China (51679067 and 51879088), and Fundamental Research Funds for the Central Universities (B200204002). The relevant data arising from this research are listed in the references, tables, and figures contained herein. Any additional details can be obtained from the corresponding author (amir.jazayeri@flinders.edu.au).

References

Alaghmand, S., Beecham, S., Jolly, I. D., Holland, K. L., Woods, J. A., & Hassanli, A. (2014), Modelling the impacts of river stage manipulation on a complex river-floodplain system in a semi-arid region. *Environmental Modelling and Software.*, *59*, 109–126. https://doi.org/10.1016/j.envsoft.2014.05.013

Alaghmand, S., Beecham, S., Woods, J. A., Holland, K. L., Jolly, I. D., Hassanli, A., & Nouri, H. (2015), Injection of fresh river water into a saline floodplain aquifer as a salt interception measure in a semi-arid environment. *Ecolological Engineering*, *75*, 308–322. https://doi.org/10.1016/j.ecoleng.2014.11.014

Cartwright, I., Weaver, T. R., Simmons, C. T., Fifield, L. K., Lawrence, C. R., Chisari, R., & Varley, S. (2010), Physical hydrogeology and environmental isotopes to constrain the age, origins, and stability of a low-salinity groundwater lens formed by periodic river recharge: Murray Basin, Australia. *Journal of Hydrology*, *380*(1-2), 203–221. https://doi.org/10.1016/j.jhydrol.2009.11.001

Cendón, D. I., Larsen, J. R., Jones, B. G., Nanson, G. C., Rickleman, D., Hankin, S. I., Pueyo, J. J., & Maroulis, J. (2010), Freshwater recharge into a shallow saline groundwater system, Cooper Creek floodplain, Queensland, Australia. *Journal of Hydrology*, *392*(3–4), 150–163. https://doi.org/10.1016/j.jhydrol.2010.08.003

Guo, W., & Langevin, C. D. (2002), *User's Guide to SEAWAT: A Computer Program For Simulation of Three-Dimensional Variable-Density Ground-Water Flow*, U.S. Geological Survey Techniques of Water-Resources Investigations. Book 6, Chapter A7, 77 pp., Tallahassee, Florida.

Haitjema, H. M. (1987), Comparing a three-dimensional and a Dupuit-Forchheimer solution for a circular recharge area in a confined aquifer. *Journal of Hydrology*, *91*, 83–101. https://doi.org/10.1016/0022-1694(87)90130-2

Hantush, M. S. (1965), Wells near Streams with Semipervious Beds. *Journal of Geophysical Research*, *70*(12), 2829–2838. https://doi.org/10.1029/JZ070i012p02829

Harbaugh, A. W., Banta, E. R., Hill, M. C., & McDonald, M. G. (2000), *MODFLOW-2000, the U. S. Geological Survey Modular Ground-Water Model - User Guide to Modularization Concepts and the Ground-Water Flow Process*, U. S. Geological Survey, Open File, 00-92, 121 pp., Reston, Virginia.

Holland, K. L., Charles, A. H., Jolly, I. D., Overton, I. C., Gehrig, S., & Simmons, C. T. (2009), Effectiveness of artificial watering of a semi-arid saline wetland for managing riparian vegetation health. *Hydrological Processes.*, *23*(24), 3474–3484. https://doi.org/10.1002/hyp.7451

Laattoe, T., Werner, A. D., Woods, J. A., & Cartwright, I. (2017), Terrestrial freshwater lenses: Unexplored subterranean oases. *Journal of Hydrology*, *553*, 501–507. https://doi.org/10.1016/j.jhydrol.2017.08.014

Langevin, C. D., Thorne Jr., D. T., Dausman, A. M., Sukop, M. C., & Guo, W. (2008), *SEAWAT Version 4: A Computer Program for Simulation of Multi-Species Solute and Heat Transport*, U. S. Geological Survey Techniques and Methods. Book 6, Chapter A22, 39 pp., Reston, Virginia.

Miracapillo, C., & Morel-Seytoux, H. J. (2014), Analytical solutions for stream-aquifer flow exchange under varying head asymmetry and river penetration: Comparison to numerical solutions and use in regional groundwater models. *Water Resources Research*, *50*(9), 7430–7444. https://doi.org/10.1002/2014WR015456

Morel-Seytoux, H. J. (1975), A Simple Case of Conjunctive Surface-Ground-Water Management. *Ground Water*, *13*(6), 506–515. https://doi.org/10.1111/j.1745-6584.1975.tb03620.x

Morel-Seytoux, H. J. (2009), The turning factor in the estimation of stream-aquifer seepage. *Ground Water*, *47*(2), 205–212. https://doi.org/10.1111/j.1745-6584.2008.00512.x

Morel-Seytoux, H. J., Mehl, S., & Morgado, K. (2014), Factors Influencing the Stream-Aquifer Flow Exchange Coefficient. *Ground Water*, *52*(5), 775–781. https://doi.org/10.1111/gwat.12112

Morel-Seytoux, H. J., Miller, C. D., Miracapillo, C. & Mehl, S. (2017), River Seepage Conductance in Large-Scale Regional Studies. *Groundwater*, *55*(3), 399–407. https://doi.org/ 10.1111/gwat.12491

Moriasi, D., Arnold, J., Van Liew, M., Bingner, R., Harmel, R., & Veith, T. (2007), Model evaluation guidelines for systematic quantification of accuracy in watershed simulations. *Transactions of the ASABE*, *50*(3), 885–900. https://doi.org/10.13031/2013.23153

Munday, T., Fitzpatrick, A., Doble, R. C., Berens, V., Hatch, M., & Cahill, K. (2006), The combined use of air, ground and 'in river' electromagnetics in defining spatial processes of salinisation across ecologically important floodplain areas: Lower River Murray, SA, In: Regolith 2006: Consolidation and Dispersion of Ideas, pp. 249–255, CRC LEME, Hahndorf, Australia. [Available at www.crcleme.org.au/Pubs/Monographs/regolith2006/Munday_T.pdf.]

Telfer, A., Burnell, R., Woods, J., & Weir, Y. (2012), River Murray floodplain salt mobilisation and salinity exceedances at Morgan, prepared by Australian Water Environments for the Murray-Darling Basin Authority, *MDBA* Pub. No. 53/12, 175.

Werner, A. D. (2017), Correction factor to account for dispersion in sharp-interface models of terrestrial freshwater lenses and active seawater intrusion. *Advances in Water Resources*, *102*, 45–52. https://doi.org/10.1016/j.advwatres.2017.02.001

Werner, A. D., & Laattoe, T. (2016), Terrestrial freshwater lenses in stable riverine settings: Occurrence and controlling factors. *Water Resources Research*, *52*(5), 3654–3662. https://doi.org/10.1002/2015wr018346

Werner, A. D., Kawachi, A., & Laattoe, T. (2016), Plausibility of freshwater lenses adjacent to gaining rivers: Validation by laboratory experimentation. *Water Resources Research*, *52*(11), 8487–8499. https://doi.org/10.1002/2016wr019400

Zheng, C., & Wang, P. P. (1999), *MT3DMS: A modular three-dimensional multispecies transport model for simulation of advection, dispersion and chemical reactions of contaminants in groundwater systems: Documentation and user's guide*, Contract Report SERDP-99-1, U.S. Army Corps of Engineers-Engineer Research and Development Center.

Notations

α_L [L]	longitudinal dispersivity
α_T [L]	transverse dispersivity
η_a [L]	depth of aquifer base below the riverbed
η_f [L]	freshwater thickness
η_r [L]	river penetration depth
η_s; η_{s1}; η_{s2} [L]	saltwater thickness (the depth of saltwater flow)
η_{sb} [-]	saltwater thickness at the landward boundary located at x_b
η_{sB} [L]	saltwater thickness at x_B
$\eta_{sB,\,Full}$ [L]	saltwater thickness at x_B for fully penetrating river
η_{sL} [L]	saltwater thickness the lens tip
η_{sr} [L]	saltwater thickness at the origin (adjacent to the riverbank)
$\eta_{sr,\,Full}$ [L]	saltwater thickness at the origin (adjacent to the riverbank) for fully penetrating river
μ_f [$ML^{-1}T^{-1}$]	freshwater dynamic viscosity
μ_s [$ML^{-1}T^{-1}$]	saltwater dynamic viscosity
ρ_f [ML^{-3}]	freshwater density
ρ_s [ML^{-3}]	saltwater density
Γ [-]	one-side dimensionless conductance
Γ_c [-]	one-side dimensionless conductance in the presence of a clogging layer
Γ_{flat} [-]	one-side dimensionless conductance in case of no penetration of the river or a flat recharge zone
Γ_p [L]	one-side dimensionless conductance in case of partial penetration of the river
Γ_s [-]	modified one-side dimensionless conductance for saltwater flow
ΔA [L^2]	cell cross-sectional area perpendicular to the flow
ΔL [L]	cell size in the direction of flow
Δx; Δy; Δz [L]	cell size in x, y and z directions, respectively
a; b; c [-]	coefficients in equation (16)
a_1; a_2 [-]	coefficients in equation (24)
B_r [L]	clogging layer (resistive material) thickness
C_{GHB} [L^2T^{-1}]	general-head boundary conductance
d [L]	average aquifer thickness

591	d_p^N [-]	normalised degree of penetration of the river (freshwater only)
592	d_s [L]	average thickness of saltwater between the riverbank and at distance x_B
593	d_{sp}^N [-]	saltwater normalised degree of penetration
594	D_m [L^2T^{-1}]	molecular diffusion
595	h_B [L]	head in the aquifer at x_B
596	h_r [L]	head in the river
597	h_s [L]	equivalent saltwater head
598	h_{sB} [L]	equivalent hydrostatic saltwater head at x_B
599	h_{sr} [L]	equivalent hydrostatic saltwater head at the river
600	K [LT^{-1}]	aquifer freshwater hydraulic conductivity
601	K_c [LT^{-1}]	clogging layer freshwater hydraulic conductivity
602	K_s [LT^{-1}]	saltwater hydraulic conductivity of the aquifer
603	K_{sc} [LT^{-1}]	saltwater hydraulic conductivity of the clogging layer
604	L [L]	river reach length (perpendicular to the river cross-section)
605	n [-]	effective porosity
606	q_s [L^2T^{-1}]	steady-state saline groundwater discharge
607	$q_{s,\,Full}$ [L^2T^{-1}]	steady-state saline groundwater discharge for fully penetrating river
608	Q [L^3T^{-1}]	fresh groundwater flow to each side of the river
609	S_y [-]	specific yield
610	S_s [L^{-1}]	specific storage
611	W_p^N [-]	normalized wetted perimeter (freshwater only)
612	W_p [L]	wetted perimeter of the river (freshwater only)
613	W_r [L]	half of the river width
614	W_{sp}^N [-]	saltwater normalised wetted perimeter
615 616	W_{sp} [L]	total wetted perimeter through which saltwater discharges (on both sides of the river)
617	x; x_1; x_2 [L]	horizontal distance from riverbank
618	x_b [L]	landward boundary distance from riverbank
619	x_B [L]	“far distance” from the river where the D-F assumption is valid
620	x_L [L]	riparian lens extent
621	$x_{L,\,Full}$ [L]	riparian lens extent for fully penetrating river

NSE	Nash-Sutcliffe efficiency
MAE	mean absolute error
RMSE	root mean square error
PBIAS	percent bias